J Sci Comput (2011) 49:3–20
DOI 10.1007/s10915-011-9464-8

Horizontal Large Eddy Simulation of Stratified Mixing in a Lock-Exchange System

Luigi C. Berselli · Paul F. Fischer · Traian Iliescu · Tamay M. Özgökmen

Received: 28 February 2010 / Revised: 27 December 2010 / Accepted: 9 January 2011 /
Published online: 19 January 2011

Abstract This paper presents analytical and numerical results for two new anisotropic modifications of the Rational and Clark-α LES models. The main difference from their standard form is that in this study horizontal (as opposed to isotropic) spatial filtering is used, which is appropriate for turbulent mixing in stratified flows. We present several mathematical results regarding the horizontal Rational and Clark-α LES models. We also present numerical experiments that support the analytical developments and show that both horizontal LES models perform better than their standard, isotropic counterparts in approximating mixing in a 3D lock-exchange problem at Reynolds number $Re = 10{,}000$.

Keywords Stratified flows · Horizontal filtering · Rational/Clark-α LES model · Boussinesq equations · LES in domains with boundary

1 Introduction

Turbulent mixing of stratified flows plays a fundamental role in the dynamics of the ocean circulation. This process is particularly important near the surface and the bottom of the

L.C. Berselli (✉)
Dipartimento di Matematica Applicata "U. Dini", Università di Pisa, Via F. Buonarroti 1/c, 56127, Pisa, Italy
e-mail: berselli@dma.unipi.it

P.F. Fischer
Argonne National Laboratory, Argonne, IL, USA
e-mail: fischer@mcs.anl.gov

T. Iliescu
Department of Mathematics, Virginia Polytechnic Institute and State University, Blacksburg, VA, USA
e-mail: iliescu@vt.edu

T.M. Özgökmen
RSMAS/MPO, University of Miami, Miami, FL, USA
e-mail: tozgokmen@rsmas.miami.edu

ocean, near topographic features, near polar and marginal seas, as well as near the equatorial zones [29, 48]. In coastal waters, turbulent mixing is important for the transport and dispersion of biological species, and coastal discharges, while in the large scale flows, the irreversible changes in the water mass properties may have implications for the meridional overturning circulation [37, 38]. One of the main challenges in representing this fundamental process in coastal and ocean general circulation models is the large range of scales in the ocean.

A promising approach in overcoming this computational challenge is *large eddy simulation (LES)*, which relies on the spatial filtering of the (non-hydrostatic) Navier-Stokes equations. LES aims at computing the large eddies, which carry out most of the mixing and transport, are inhomogeneous, long-lived, depend on model geometry and are thus difficult to model analytically. On the other hand, the smaller eddies are more isotropic, homogeneous, short-lived, universal and can thus be modeled. Since the resolution of the smallest scales is avoided, the computational cost of LES can be several orders of magnitude less than that of *direct numerical simulation (DNS)*, in which all dynamical scales of motion are computed. Numerous LES modeling strategies have been used in the numerical simulation of mixing in stratified flows. A survey of these LES models is beyond the scope of this report; the interested reader is referred to, e.g., [1, 30, 36, 41].

This report puts forth two *new* LES models for the numerical simulation of mixing in stratified flows: the horizontal Rational LES model and the horizontal Clark-α LES model. The starting point in the development of these two new LES models is represented by the isotropic Rational LES model [20] and Clark-α LES model [11]. We mention that both isotropic models have already been used in the numerical simulation of stratified flows and have compared favorably to state-of-the-art LES models, such as the dynamic subgrid-scale LES model [40–42]. The new horizontal LES models (which were announced in [6]), utilize *horizontal spatial filtering* instead of the usual isotropic spatial filtering employed in the derivation of the original Rational and Clark-α LES models. We emphasize that, although the idea of anisotropic filtering has been employed before, the connection with LES based on wave number approximation and with the family of α-models, together with the treatment of boundary conditions is, to the best of our knowledge, original. The main goal of this report is to investigate both theoretically and numerically the new horizontal Rational and Clark-α LES models. We also take the opportunity of giving more mathematical details on the analytical properties of horizontal filtering, and explain why it seems appealing from the computational point of view.

One of the well-known features of mixing in stratified flows is that filtering seems to be required only in the horizontal directions, because mixing takes place mainly along these two directions. Another justification for the use of partial (horizontal) viscosities and/or filtering comes from the study of Ekman boundary layers for rotating fluids. Indeed, in [13] and references therein, the system of the Navier-Stokes equations with horizontal viscosity was considered. These are the main modeling motivations for the two new horizontal LES models that we study. We also emphasize that the two new horizontal LES models do not need artificial boundary conditions in the vertical direction. Thus, one of the main hurdles in the development of robust LES modeling strategies is circumvented.

The horizontal Rational and Clark-α LES models are evaluated in a 3D *lock-exchange problem*, which contains shear-driven mixing, internal waves, interactions with boundaries and convective motions, while having a simple domain, initial and boundary conditions, and forcing. Instead of taking the more conventional route of applying LES in an oceanographic setting and comparing with observational results, we set up a canonical benchmark problem, the lock-exchange problem in an enclosed box domain. In this problem, the vertical barrier

separating two fluids of different densities is abruptly removed, and counter-propagating gravity currents initiate mixing via shear. The time evolution of the lock-exchange problem in an enclosed domain is quite complex, showing shear-driven mixing, internal waves interacting with the flow field and the solid boundaries, gravitationally-unstable phases and flow transients. Yet, the problem involves simple and unambiguous forcing, initial and boundary conditions. The rationale for our choice is that, in oceanic cases, the scarcity of observations and the uncertainties due to sampling errors of measurements, forcing, initialization, and boundary conditions can obscure the effect of LES modeling. The lock-exchange setup has long served as a paradigm configuration for studying the spatiotemporal evolution of gravity currents. This benchmark problem has been investigated both experimentally [8, 22–24, 26, 44, 46] and theoretically [2, 45]. The direct numerical simulations in [9, 10, 25] provided detailed information on the dynamics of the lock-exchange problem. The impressive amount of data and the physical relevance of the lock-exchange problem make it an appropriate benchmark and a natural first step in the thorough assessment of the performance of the new horizontal Rational and Clark-α LES models.

2 The Horizontal Rational and Clark-α LES Models

To a first approximation, the mixing phenomena can be described mathematically by means of the Boussinesq system of partial differential equations:

$$\begin{aligned} &\partial_t \mathbf{u} + \nabla\cdot(\mathbf{u}\otimes\mathbf{u}) - \frac{1}{Re}\Delta\mathbf{u} + \nabla p = -\frac{1}{Fr^2}\rho'\mathbf{e}_3, \quad \text{with } \nabla\cdot\mathbf{u} = 0, \\ &\partial_t \rho' + \nabla\cdot(\rho'\mathbf{u}) - \frac{1}{Re\,Pr}\Delta\rho' = 0. \end{aligned} \tag{1}$$

The unknowns $(\mathbf{u}, p, \rho')$ are velocity, pressure, and "salinity perturbation," respectively, and $\mathbf{e}_3 = (0, 0, 1)$. The non-dimensional parameters are the Reynolds number Re, the Prandtl number Pr, and the Froude number Fr.

The problem we consider takes place naturally in an elongated domain:

$$D := \{x \in \mathbb{R}^3 : -\pi < x_1, x_2 < \pi,\ -d < x_3 < d\} \quad \text{with } d \ll 1.$$

The boundary $\partial D := \{x \in \mathbb{R}^3 : -\pi < x_1, x_2 < \pi, x_3 = \pm d\}$ is flat and we enforce periodic boundary conditions on the "*horizontal variables*" $x_h := (x_1, x_2)$. We use the subscript "$_h$" to denote differential operators acting only on the horizontal variables, and we write $\Delta_h := \partial^2_{x_1} + \partial^2_{x_2}$ and $\nabla_h := (\partial_{x_1}, \partial_{x_2})$.

Since in many instances a phenomenology *à la* Kolmogorov is not available, the use of eddy viscosity methods is not completely justified. Thus, we prefer to consider herein LES methods based on wave-number asymptotics. (A review on this whole family of methods can be found in [5, Chap. 7].) The oldest such method is the "Gradient" one (known also as Taylor or Clark method and introduced in [32]) with the subfilter-scale stress tensor $\boldsymbol{\tau}_{\mathrm{G}}(\mathbf{w}, \mathbf{w}) = \frac{\alpha^2}{2}\nabla\mathbf{w}\nabla\mathbf{w}^T$, where $[\nabla\mathbf{w}\nabla\mathbf{w}^T]_{ij} := \sum_{k=1}^3 \partial_{x_k} w_i \partial_{x_k} w_j$ and α is the spatial filter radius. It is well-known that instabilities occur in the numerical implementation and that some kind of smoothing must be added in order to have effective simulations, see, e.g., [21]. Filtered versions of the Gradient model yield the *Rational* and *Clark-α LES models*, whose subfilter-scale stress tensors read: $\boldsymbol{\tau}_{\mathrm{R}}(\mathbf{w}, \mathbf{w}) = (\mathrm{I} - \frac{\alpha^2}{4}\Delta)^{-1}\frac{\alpha^2}{2}\nabla\mathbf{w}\nabla\mathbf{w}^T$ and $\boldsymbol{\tau}_{\mathrm{C}}(\mathbf{w}, \mathbf{w}) = (\mathrm{I} - \frac{\alpha^2}{2}\Delta)^{-1}\frac{\alpha^2}{2}\nabla\mathbf{w}\nabla\mathbf{w}^T$, respectively. We note that the two LES models also

involve a shape parameter $\gamma > 0$, which is related to the particular spatial filtering utilized. The Rational LES model has been derived by a rational approximation of wave-numbers, while the Clark-α LES model is based on analogies with the Helmholtz filtering. The mathematical analysis of these models can be found in [4, 11], while a subtle -but elementary- mathematical difference between the two methods is pointed out in [6].

2.1 Derivation of the Horizontal Rational and Clark-α LES Models

To derive the horizontal Rational and Clark-α LES models, we adapt the approach of [20, 32]. To this end, we consider smoothing acting only on the horizontal variables, which can be performed by means of convolution with the following kernel: $g_\alpha(x) = \frac{1}{\pi\alpha^2}\,\mathrm{Exp}(-\frac{x_1^2+x_2^2}{\alpha^2})$. For simplicity, in this section we set the shape parameter $\gamma = 1$. By taking the 2D Fourier transform with respect to x_h and denoted by $\mathcal{F}_h$, one gets $\mathcal{F}_h(g_\alpha)(k) = \mathrm{Exp}(-\frac{\alpha^2}{4}\,({k_1}^2 + {k_2}^2))$. In a standard way, by setting $\overline{u} = g_\alpha * u$ and $u' = u - \overline{u}$, we observe that $\mathcal{F}_h(\overline{u})(k) = \mathcal{F}_h(g_\alpha)(k)\mathcal{F}_h(\overline{u})(k) + \mathcal{F}_h(g_\alpha)(k)\mathcal{F}_h(u')(k)$, and we can write

$$\mathcal{F}_h(u')(k) = \left(\frac{1}{\mathcal{F}_h(g_\alpha)(k)} - 1\right)\mathcal{F}_h(\overline{u})(k).$$

This implies the following identities:

$$\begin{aligned}
&\mathcal{F}_h(\overline{\overline{u}_i\,\overline{u}_j})(k) = \mathcal{F}_h(g_\alpha)(k)\,\mathcal{F}_h(\overline{u}_i)(k) * \mathcal{F}_h(\overline{u}_j)(k),\\
&\mathcal{F}_h(\overline{\overline{u}_i\,u'_j})(k) = \mathcal{F}_h(g_\alpha)(k)\,\mathcal{F}_h(\overline{u}_i)(k) * \left[\left(\frac{1}{\mathcal{F}_h(g_\alpha)(k)} - 1\right)\mathcal{F}_h(\overline{u}_j)(k)\right],\\
&\mathcal{F}_h(\overline{u'_i\,\overline{u}_j})(k) = \mathcal{F}_h(g_\alpha)(k)\left[\left(\frac{1}{\mathcal{F}_h(g_\alpha)(k)} - 1\right)\mathcal{F}_h(\overline{u}_i)(k)\right] * \mathcal{F}_h(\overline{u}_j)(k),\\
&\mathcal{F}_h(\overline{u'_i\,u'_j})(k) = \mathcal{F}_h(g_\alpha)(k)\left[\left(\frac{1}{\mathcal{F}_h(g_\alpha)(k)} - 1\right)\mathcal{F}_h(\overline{u}_i)(k)\right]\\
&\qquad\qquad * \left[\left(\frac{1}{\mathcal{F}_h(g_\alpha)(k)} - 1\right)\mathcal{F}_h(\overline{u}_j)(k)\right].
\end{aligned}$$

By inserting the Taylor series expansion for $\mathcal{F}_h(g_\alpha)(k)$

$$\mathcal{F}_h(g_\alpha)(k) = 1 - \frac{\alpha^2}{4}|k|^2 + O(\alpha^4) \quad \text{and} \quad \frac{1}{\mathcal{F}_h(g_\alpha)(k)} - 1 = \frac{\alpha^2}{4}|k|^2 + O(\alpha^4)$$

in the previous formulas, and with the standard properties of the Fourier transform, one *formally* obtains:

$$\overline{\overline{u}_i\,\overline{u}_j} = \overline{u}_i\,\overline{u}_j + \frac{\alpha^2}{4}\Delta_h(\overline{u}_i\,\overline{u}_j) + O(\alpha^4), \qquad \overline{\overline{u}_i\,u'_j} = -\frac{\alpha^2}{4}\overline{u}_i\,\Delta_h\overline{u}_j + O(\alpha^4),$$

$$\overline{u'_i\,\overline{u}_j} = -\frac{\alpha^2}{4}\Delta_h\overline{u}_i\,\overline{u}_j + O(\alpha^4), \qquad \overline{u'_i\,u'_j} = O(\alpha^4).$$

Using these formulas and disregarding the terms formally of higher order (in α), leads to the following expression for the subfilter-scale tensor for the *horizontal version of the Gradient LES model:*

$$\boldsymbol{\tau}_{\mathrm{hG}}(\mathbf{w},\mathbf{w}) = \frac{\alpha^2}{2}\nabla_h\mathbf{w}\nabla_h\mathbf{w}^T,$$

where $[\nabla_h \mathbf{w} \nabla_h \mathbf{w}^T]_{ij} := \sum_{k=1}^{2} \partial_{x_k} w_i \partial_{x_k} w_j$.

Following the same approach as above and using the following expansion based on the $(0, 1)$-Padé approximation of the exponential

$$\mathcal{F}_h(g_\alpha)(k) = \frac{1}{1 + \frac{\alpha^2}{4}|k|^2} + O(\alpha^4), \qquad \frac{1}{\mathcal{F}_h(g_\alpha)(k)} - 1 = \frac{\alpha^2}{4}|k|^2 + O(\alpha^4),$$

we get:

$$\overline{\overline{u}_i\,\overline{u}_j} = \left(\mathrm{I} - \frac{\alpha^2}{4}\Delta_h\right)^{-1} \overline{u}_i\,\overline{u}_j, \qquad \overline{\overline{u}_i\,u'_j} = -\frac{\alpha^2}{4}\left(\mathrm{I} - \frac{\alpha^2}{4}\Delta_h\right)^{-1} \overline{u}_i\,\Delta_h\overline{u}_j,$$

$$\overline{u'_i\,\overline{u}_j} = -\frac{\alpha^2}{4}\left(\mathrm{I} - \frac{\alpha^2}{4}\Delta_h\right)^{-1} \Delta_h\overline{u}_i\,\overline{u}_j, \qquad \overline{u'_i\,u'_j} = \frac{\alpha^4}{16}\left(\mathrm{I} - \frac{\alpha^2}{4}\Delta_h\right)^{-1} \Delta_h\overline{u}_i\,\Delta_h\overline{u}_j.$$

Substitution into the averaged equations and some algebraic manipulations finally yield the subfilter-scale stress tensor for the *horizontal Rational LES model*:

$$\boldsymbol{\tau}_{\mathrm{hR}}(\mathbf{w}, \mathbf{w}) = \left(\mathrm{I} - \frac{\alpha^2}{4}\Delta_h\right)^{-1} \frac{\alpha^2}{2}\nabla_h \mathbf{w} \nabla_h \mathbf{w}^T.$$

In analogy to Helmholtz filtering of the horizontal Gradient model, one also obtains the subfilter-scale stress tensor for the *horizontal Clark-α LES model*:

$$\boldsymbol{\tau}_{\mathrm{hC\text{-}}\alpha}(\mathbf{w}, \mathbf{w}) = \left(\mathrm{I} - \frac{\alpha^2}{2}\Delta_h\right)^{-1} \frac{\alpha^2}{2}\nabla_h \mathbf{w} \nabla_h \mathbf{w}^T.$$

The advantage of the horizontal Rational and Clark-α LES models over their isotropic counterparts is obvious: From the computational point of view, the inversion of a horizontal Laplacian is *significantly more efficient* than the inversion of the isotropic one. Another major advantage of the horizontal LES models is that *there is no need* to introduce extra/artificial boundary conditions for the Helmholtz operator in the vertical direction. Indeed, one can simply use $\mathbf{w} = \mathbf{u}$ in the vertical x_3-direction.

To simplify notation, in what follows we consider the *horizontal Rational/Clark-α LES model*:

$$\partial_t \mathbf{w} + \nabla \cdot (\mathbf{w} \otimes \mathbf{w}) - \frac{1}{Re}\Delta \mathbf{w} + \nabla \cdot \left(\mathrm{I} - \kappa\frac{\alpha^2}{4\gamma}\Delta_h\right)^{-1} \frac{\alpha^2}{2\gamma}\nabla_h \mathbf{w} \nabla_h \mathbf{w}^T + \nabla q = \mathbf{f}, \qquad (2)$$

with $\nabla \cdot \mathbf{w} = 0$. In (2), γ is the shape parameter, and $\kappa = 1$ yields the horizontal Rational LES model, while $\kappa = 2$ yields the horizontal Clark-α LES model. As explained in [6], the different value of the constant κ is responsible for rather different mathematical properties.

It seems that the subfilter-scale stress and the viscous term in (2) have different forms. Indeed, the viscous term retains its original 3D form, whereas the LES model displays the horizontal filtering operation. This difference, however, is only in form, since the Laplace operator in the viscous term is applied to $\mathbf{w}$, which is the *horizontally filtered* velocity. Thus, both the viscous term and the LES model in (2) include the horizontal filtering operation, the former implicitly (through $\mathbf{w}$), and the latter explicitly. The reason for the dependence on the horizontal filter is displayed explicitly in the LES model and is due to the nonlinear term $\nabla \cdot (\mathbf{w} \otimes \mathbf{w})$; since the Laplacian is linear, the differentiation and filtering operators commute, and thus the only dependence on horizontal filtering in the viscous term is through $\mathbf{w}$.

2.2 Mathematical Properties of the Horizontal Rational and Clark-α LES Models

In this section, we present several mathematical results that are closely related to the horizontal filtering employed in the derivation of the horizontal Rational and Clark-α LES models. Of special practical significance is the result in Proposition 1, which shows that the Helmholtz and Helmholtz-Stokes operators are the same in our setting. We also prove in Theorem 2 the precise energy balance of the horizontal Rational and Clark-α LES models. From a practical point of view, this theoretical result allows us to interpret the possible divergence of the numerical solution as a consequence of an inadequate numerical algorithm, and not of potentially inadequate modeling. We emphasize that we only sketch the proofs of the theoretical results presented in this section; for more details (including alternative LES modeling strategies), the reader is referred to [3].

We start by giving some mathematical details on the horizontal filter, in order to show: (i) the appropriate treatment of its boundary conditions, and (ii) its relation to the Helmholtz filter. Given a vector field $\mathbf{f}$, an "averaged" field $\mathbf{u}$ is defined by solving the following *horizontal Helmholtz-Stokes* problem:

$$\begin{aligned} \mathbf{u} - \alpha^2 \Delta_h \mathbf{u} + \nabla p &= \mathbf{f} \quad \text{in } D, \\ \nabla \cdot \mathbf{u} &= 0 \quad \text{in } D, \\ \mathbf{u} \cdot \mathbf{n} &= 0 \quad \text{on } \partial D, \end{aligned} \tag{3}$$

where here and throughout the paper $\alpha > 0$ will be a fixed constant (the spatial filter radius). We use the notation

$$L^2(D) := \left\{ \phi : D \to \mathbb{R},\ x_h\text{-periodic, measurable, with } \int_D |\phi|^2 dx < +\infty \right\},$$

$L^2_0 \subset L^2(D)$ denotes the space of functions in $L^2(D)$ with vanishing mean value, and $\mathbb{L}^2 := (L^2(D))^3$. We use the same symbol $\|\cdot\|$ for the norm in these spaces, and we define the following space:

$$\mathbb{H}^1_h := \left\{ \mathbf{u} \in L^2 : \nabla_h \mathbf{u} \in (L^2(D))^6,\ \nabla \cdot \mathbf{u} \in L^2(D),\ \mathbf{u} \cdot \mathbf{n} = 0 \text{ in } H^{-1/2}(\partial D) \right\},$$

where $\mathbf{n}$ denotes the exterior unit normal vector on ∂D. Note that, since $\mathbf{u}$ has divergence in $L^2(D)$, we have $\frac{\partial u_3}{\partial x_3} = -\nabla_h \cdot \mathbf{u}_h = -\frac{\partial u_1}{\partial x_1} - \frac{\partial u_2}{\partial x_2} \in L^2(D)$. This shows that some extra-regularity for the vertical component of the velocity is obtained for free.

Theorem 1 *Let $\mathbf{f} \in \mathbb{L}^2$ and $\alpha > 0$. Then, there exists a unique $(\mathbf{u}, p) \in \mathbb{H}^1_h \times L^2_0$ solution of (3) and a constant $c = c(\alpha)$, such that*:

$$\|\mathbf{u}\| + \alpha \|\nabla_h \mathbf{u}\| + \alpha \|\nabla u_3\| + \|p\| \le c \|\mathbf{f}\|.$$

Moreover, the weak solution $(\mathbf{u}, p)$ is smoother and satisfies:

$$\|\nabla_h \mathbf{u}\| + \alpha \|\nabla_h \nabla_h \mathbf{u}\| + \alpha \|\nabla \nabla_h u_3\| + \|\nabla p\| \le c \|\mathbf{f}\|.$$

Proof We follow an approach similar to that of adding some artificial compressibility. Thus, for $\lambda > 0$, we study the following problem:

$$\begin{aligned} \mathbf{u} - \alpha^2 \Delta_h \mathbf{u} - \lambda \nabla(\nabla \cdot \mathbf{u}) + \nabla p &= \mathbf{f} \quad \text{in } D, \\ \lambda p + \nabla \cdot \mathbf{u} &= 0 \quad \text{in } D, \\ \mathbf{u} \cdot \mathbf{n} &= 0 \quad \text{on } \partial D. \end{aligned}$$

Let us define the linear space $\mathbb{X} := (H_h^1)^2 \times H_0^1 \times L_0^2$. On $\mathbb{X}^2$, we define the family of bi-linear forms (parametrized by $\lambda > 0$)

$$a_\lambda(U, V) := \int_D \mathbf{u} \cdot \mathbf{v}\, dx + \alpha^2 \int_D \nabla_h \mathbf{u} : \nabla_h \mathbf{v}\, dx + \mu \int_D (\nabla \cdot \mathbf{u})(\nabla \cdot \mathbf{v})\, dx$$
$$- \int_D p\, (\nabla \cdot \mathbf{v})\, dx + \lambda \int_D p\, q\, dx + \int_D (\nabla \cdot \mathbf{u})\, q\, dx,$$

for $U = (\mathbf{u}, p)$ and $V = (\mathbf{v}, q)$. The bi-linear form $a_\lambda(\cdot, \cdot)$ is continuous and also coercive in $\mathbb{X}^2$, since

$$a_\lambda(U, U) = \int_D |\mathbf{u}|^2\, dx + \alpha^2 \int_D |\nabla_h \mathbf{u}|^2\, dx + \mu \int_D |\nabla \cdot \mathbf{u}|^2 + \lambda \int_D |p|^2\, dx,$$

and the latter quantity is equivalent to the norm of $\mathbb{X}$. By using Lax-Milgram lemma (cf. [7]), for each $\mathbf{f} \in \mathbb{L}^2$ there exists a unique solution $U_\lambda = (\mathbf{u}_\lambda, p_\lambda) \in \mathbb{X}$ of the variational problem

$$\text{find} \quad U_\lambda = (\mathbf{u}_\lambda, p_\lambda) \in \mathbb{X} : \quad a_\lambda(U_\lambda, V) = \int_D \mathbf{f}\mathbf{v}\, dx \quad \forall V = (\mathbf{v}, q) \in \mathbb{X}.$$

Moreover, the following estimate is obtained using U_λ as test function:

$$\frac{\|\mathbf{u}_\lambda\|^2}{2} + \alpha^2 \|\nabla_h \mathbf{u}_\lambda\|^2 + \lambda \|\nabla \cdot \mathbf{u}_\lambda\|^2 + \lambda \|p_\lambda\|^2 \le \frac{\|\mathbf{f}\|^2}{2}. \tag{4}$$

This gives immediately estimates which are valid (but not uniform) for each fixed $\lambda > 0$. Next, observe that, in the sense of distributions

$$\nabla p_\lambda = \mathbf{f} - \mathbf{u}_\lambda + \alpha^2 \Delta_h \mathbf{u}_\lambda - \lambda \nabla(\nabla \cdot \mathbf{u}_\lambda).$$

Denoting by $H^{-1} = (H_0^1(D))^*$ (the topological dual of $H_0^1(D)$, the space of functions vanishing on the boundary and with distributional first order derivatives in $L^2(D)$), we get by comparison:

$$\|\nabla p_\lambda\|_{H^{-1}} \le \|\mathbf{f}\|_{H^{-1}} + \|\mathbf{u}_\lambda\|_{H^{-1}} + \alpha^2 \|\Delta_h \mathbf{u}_\lambda\|_{H^{-1}} + \lambda \|\nabla(\nabla \cdot \mathbf{u}_\lambda)\|_{H^{-1}}.$$

Next, we observe that $\|\mathbf{f}\|_{H^{-1}} \le C\|\mathbf{f}\|$ and $\|\Delta_h \mathbf{u}_\lambda\|_{H^{-1}} \le C\|\nabla_h \mathbf{u}_\lambda\|$. A similar estimate also holds for the last term. Hence, by using the well-known inequality

$$\exists c > 0 \quad \|f\|_{L^2} \le c \|\nabla f\|_{H^{-1}}, \quad \text{valid for all } f \in L_0^2,$$

we obtain that

$$\|p_\lambda\| \le c \|\nabla p_\lambda\|_{H^{-1}} \le c\big(\|\mathbf{f}\| + \|\mathbf{u}_\lambda\| + \alpha^2 \|\nabla_h \mathbf{u}_\lambda\| + \lambda \|\nabla \cdot \mathbf{u}_\lambda\|\big). \tag{5}$$

Adding the square of the latter inequality to both sides of (4), recalling that from (4) the right-hand side of (5) is bounded uniformly in terms of the data, and with the Schwartz inequality, we easily obtain

$$\frac{\|\mathbf{u}_\lambda\|^2}{2} + \alpha^2 \|\nabla_h \mathbf{u}_\lambda\|^2 + \lambda \|\nabla \cdot \mathbf{u}_\lambda\|^2 + \left(\frac{1}{2} + \lambda\right) \|p_\lambda\|^2 \le c \|\mathbf{f}\|^2.$$

The now uniform bounds in $\lambda > 0$ allow to find a sequence $\lambda_n \to 0$ and a function $U = (\mathbf{u}, p) \in (H_h^1)^3 \times L_0^2$ such that

$$\mathbf{u}_{\lambda_n} \overset{weakly}{\to} \mathbf{u} \quad \text{in } (H_h^1)^3 \quad \text{and} \quad p_{\lambda_n} \overset{weakly}{\to} p \quad \text{in } L_0^2.$$

Moreover, since in the sense of distributions we have $\nabla \cdot \mathbf{u}^\lambda = -\lambda\, p_\lambda$, it also follows that $\|\nabla \cdot \mathbf{u}^\lambda\|$ is bounded uniformly. Consequently (up to a sub-sequence) we can find $\lambda_n \to 0$ such that

$$\mathbf{u}_{\lambda_n} \overset{weakly}{\to} \mathbf{u} \quad \text{in } \mathbb{H}_h^1 \quad \text{and} \quad p_{\lambda_n} \overset{weakly}{\to} p \quad \text{in } L_0^2.$$

By passing to the limit in the variational formulation, we obtain that $(\mathbf{u}, p) \in \mathbb{X}$ is the unique solution of the problem with $\lambda = 0$, with the requested estimate in terms of $\mathbf{f}$ and α. The further regularity property follows by standard tools with Nirenberg translations method (see [3] for further details). □

The previous result has an important computational consequence: In our setting the Helmholtz and Helmholtz-Stokes problem are the same, as it happens in the space-periodic case. This follows from Proposition 1 below and motivates the name Helmholtz-Stokes. In particular, in what follows, the operator $(\mathrm{I} - \alpha^2 \Delta_h)^{-1}$ appearing in all the equations will always be the *Helmholtz* operator.

Proposition 1 *Let $\mathbf{f} \in L^2(D)$ with $\nabla \cdot \mathbf{f} = 0$ in D and $\mathbf{f} \cdot \mathbf{n} = 0$ on ∂D. Then, the pressure p in the weak solution $(\mathbf{u}, p)$ of problem (3) is identically zero.*

Proof Due to the regularity proved in the previous theorem, the calculations we perform are completely justified and not only formal. Taking the divergence of the first equation in (3), we get

$$\Delta p = 0 \quad \text{in } H^{-1},$$

since $\nabla \cdot \mathbf{u} = 0$ in $L^2(D)$ and also $\nabla \cdot (\Delta_h \mathbf{u}) = 0$ in H^{-1}. The latter follows since $\Delta_h \mathbf{u} \in \mathbb{L}^2$ and performing suitable integration by parts

$$\langle \nabla \cdot \Delta_h \mathbf{u}, \phi \rangle = -\int_D \Delta_h \mathbf{u} \nabla \phi \, dx = \int_D \nabla_h \mathbf{u} \nabla \nabla_h \phi \, dx = -\int_D \nabla_h (\nabla \cdot \mathbf{u}) \nabla_h \phi \, dx = 0.$$

Next, taking the scalar product with $\mathbf{n}$ on ∂D, we get $\partial p / \partial \mathbf{n} = 0$, hence the pressure $p \in H^1(D) \cap L_0^2$ solves (weakly) the homogeneous Neumann problem

$$\begin{cases} \Delta p = 0 & \text{in } D, \\ \dfrac{\partial p}{\partial \mathbf{n}} = 0 & \text{on } \partial D, \end{cases}$$

whose unique solution is $p = 0$. □

What is most important for the understanding of the mathematical properties of solutions of (2) is the following lemma, which is again based on suitable integration by parts (cf. [4, 11]). Its proof is given in [6].

Lemma 1 *For all sufficiently smooth vector fields* $\mathbf{w}$ *on* D, x_h*-periodic, such that* $\nabla \cdot \mathbf{w} = 0$ *in* D *and* $\mathbf{w} \cdot \mathbf{n} = 0$ *on* ∂D, *the following equality holds*:

$$\int_D \left[\nabla \cdot (\mathbf{w} \otimes \mathbf{w}) + \nabla \cdot (\mathrm{I} - \alpha^2 \Delta_h)^{-1} \alpha^2 \nabla_h \mathbf{w} \nabla_h \mathbf{w}^T\right] \cdot (\mathrm{I} - \alpha^2 \Delta_h)\mathbf{w}\, dx = 0.$$

The main result concerning system (2) with $\kappa = 2$ is the following.

Theorem 2 *Let* $\mathbf{w}_0 \in \mathbb{H}^1_h$ *and* $\mathbf{f} \in L^2(0, T; L^2)$. *Then, there exists a solution* $\mathbf{w}$ (x_h*-periodic and vanishing on* ∂D) *in the sense of distributions to system* (2), *such that*:

$$\mathbf{w}, \nabla_h \mathbf{w}, \nabla w_3 \in L^\infty(0, T; L^2) \cap L^2(0, T; H^1). \tag{6}$$

Proof We only prove the energy balance, which, together with the usual Galerkin method, can then be used to prove existence of solutions. By performing certain integrations by parts (possible by x_h-periodicity), we get the following *a priori* inequality for $\mathbf{w}$:

$$\frac{1}{2}\frac{d}{dt}\left(\|\mathbf{w}\|^2 + \alpha^2 \|\nabla_h \mathbf{w}\|^2\right) + \frac{1}{Re}\left(\|\nabla \mathbf{w}\|^2 + \alpha^2 \|\nabla \nabla_h \mathbf{w}\|^2\right) \le c\|\mathbf{f}\|^2.$$

Standard arguments, see, *e.g.*, [14], can then be used to prove that a solution exists. Regularity of w_3 follows from $\nabla \cdot \mathbf{w} = 0$. □

Remark 1 The solution $\mathbf{w}$ of (2) has regularity properties which lie "in between" those of weak and strong solutions for the NSE. (In particular, we are missing the control of $\partial_{x_3}\mathbf{w}$ in $L^\infty(0, T; L^2)$.) Consequently, we are not able to prove uniqueness within this class of solutions. In addition, one cannot start a bootstrapping argument to improve the regularity of $\mathbf{w}$: By using as test function $(\mathrm{I} - \alpha^2 \Delta_h)^2 \mathbf{w}^m$ (the counterpart of the H^2-estimates in [11]), one does not get good *a priori* estimates. Roughly speaking, it seems that multipliers that are good for $\nabla \cdot (\mathbf{w} \otimes \mathbf{w})$ are not good for $\nabla \cdot (\mathrm{I} - \frac{\alpha^2}{2}\Delta)^{-1} \alpha^2 \nabla_h \mathbf{w} \nabla_h \mathbf{w}^T$ and *vice-versa*. Based on these observations, we think that the Rational/Clark-α model (2) is probably not the best fit (at least from the point of view of uniqueness and stability of solutions) for horizontal filtering. Indeed, better theoretical results can be proved in the framework of approximate deconvolution models, *à la* Stolz & Adams, see [3, 31, 47]. The special expression of the subfilter-scale stress tensor in these models allows us to prove uniqueness, using the same multiplier and just the regularity in (6).

2.3 The Horizontal Rational and Clark-α LES Models for the Boussinesq System

In this section, we extend the horizontal Rational/Clark-α model (2) to the Boussinesq system (1). The *Boussinesq horizontal Rational/Clark-*α LES model reads:

$$\begin{aligned} &\partial_t \mathbf{w} + \nabla \cdot (\mathbf{w} \otimes \mathbf{w}) - \frac{1}{Re}\Delta \mathbf{w} + \nabla \cdot \left(\mathrm{I} - \kappa \frac{\alpha^2}{4\gamma}\Delta_h\right)^{-1} \frac{\alpha^2}{2\gamma} \nabla_h \mathbf{w} \nabla_h \mathbf{w}^T \\ &\quad + \nabla q = -\frac{1}{Fr^2}\rho' \mathbf{e}_3, \\ &\partial_t \rho' + \nabla \cdot (\rho' \mathbf{w}) - \frac{1}{Re\, Pr}\Delta \rho' = 0. \end{aligned} \tag{7}$$

We note that in (7), the velocity equation is filtered, while that for the salinity is kept unchanged. The main motivation for our approach is that in [6, 41] we have investigated many different types of subfilter-scale models for the density perturbation equation in the numerical simulation of the lock-exchange problem and found no significant influence on the mixing curve quantified by the background potential background energy. Thus, in those studies, we concluded that what really matters for mixing is the subfilter-scale stress tensor for momentum, which is the focus of the present report. Furthermore, a mathematical motivation for our choice is given by the results in [17], where it was shown that, for nonzero viscosity and vanishing diffusivity, the classical conditions which ensure regularity of the Navier-Stokes equations imply the continuation of smooth solutions of (1). In particular, in regimes where the velocity is under control in scaling invariant norms, the Boussinesq coupled system has smooth solutions as well.

With the same Galerkin approach of Sect. 2.2, one can prove the following result concerning the solution of the Boussinesq horizontal Rational/Clark-α LES model (7):

Theorem 3 *Let* $(\mathbf{w}_0, \rho_0') \in \mathbb{H}_h^1 \times L^2$. *Then, there exists a weak solution to* (7) (x_h*-periodic and with* $\mathbf{w}$, ρ' *vanishing on* ∂D) *such that*

$$\mathbf{w}, \nabla_h \mathbf{w}, \nabla w^3, \rho' \in L^\infty(0, T; L^2) \cap L^2(0, T; H^1).$$

The proof is based on the following *a priori* estimate (obtained by using as test function $((\mathrm{I} - \alpha^2 \Delta_h)\mathbf{w}, \rho')$ and by performing some integrations by parts):

$$\frac{1}{2}\frac{d}{dt}\left(\|\mathbf{w}\|^2 + \alpha^2\|\nabla_h \mathbf{w}\|^2 + \|\rho'\|^2\right) + \frac{1}{Re}\left(\|\nabla \mathbf{w}\|^2 + \alpha^2\|\nabla \nabla_h \mathbf{w}\|^2\right) + \|\nabla \rho'\|^2 \leq c(\|\rho'\|^2 + \|\mathbf{f}\|^2).$$

Thus, the energy balance of the Boussinesq horizontal Rational/Clark-α LES model (7) appears satisfactory.

3 Numerical Results

In this section, we investigate how the Boussinesq horizontal Rational/Clark-α LES models (7) perform in the numerical simulation of 3D turbulent stratified flows. To this end, we compare the performance of four LES models: (1) the isotropic Rational LES model; (2) the isotropic Clark-α LES model; (3) the horizontal Rational LES model; and (4) the horizontal Clark-α LES model—against DNS results. The comparison criterion is simple: the closer the LES results are to the benchmark DNS results, the better the LES model. To ensure a fair assessment of the performance of the LES models, we also included under-resolved numerical simulations without any LES modeling, which we denoted by DNS*. Thus, it is expected that the LES models produce results that are, *at the very least*, better than the DNS* results.

All four LES models are tested on the lock-exchange problem, a popular benchmark problem for the numerical investigation of mixing in stratified flows [10, 25, 40–42]. The model setup is similar to that in [42], which contains a detailed discussion of the boundary conditions, initial conditions and parameters used. We now briefly list them; for more details, the reader is referred to [42].

3.1 Numerical Model

The numerical study is conducted by using Nek5000, a spectral element code [18, 34, 43] that was developed by Paul Fischer and his group. Nek5000 has been already used in the numerical investigation of various LES models in homogeneous flows [27, 28], stratified flows [40, 41], and bottom gravity currents [39]. These results have formed the basis of refined parameterizations of gravity current mixing for an ocean general circulation model [12, 52].

The time advancement of the Boussinesq equations (1) is effected by using second-order semi-implicit operator-splitting methods [18, 35]. The hydrodynamics are advanced first, with explicit treatment of the buoyancy forcing term, followed by the update of the density perturbation transport. Spatial discretization is based on the spectral element method, which is a high-order weighted residual technique based on compatible velocity and pressure spaces free of spurious modes. Locally, the spectral element mesh is structured, with the solution, data, and geometry expressed as sums of Nth-order Lagrange polynomials on tensor-products of Gauss-Lobatto-Legendre (GLL) quadrature points. Globally, the mesh is an unstructured array of K deformed hexahedral elements and can include geometrically nonconforming elements. For problems having smooth solutions, the spectral element method achieves exponential convergence with N, despite having only C^0 continuity (which is advantageous for parallelism). The convection operator exhibits minimal numerical dissipation and dispersion, which is critical for high Reynolds number applications, such as that we consider in this study. For the sparse linear solvers, Nek5000 employs as a preconditioner the additive overlapping Schwarz method [16, 18, 33], which uses fast local solvers that exploit the tensor-product form and a parallel coarse-grid solver that scales to thousands of processors [50].

The nonlinear advection term $\nabla \cdot (\mathbf{u} \otimes \mathbf{u})$ in the Boussinesq equations (1) generates energy at high wave numbers that cannot be captured on the mesh. This can lead to an accumulation of energy at smaller scales. To help achieve numerical stability at high Re without compromising the solution accuracy, the following two approaches are used in Nek5000: The first method is dealiasing through the 3/2 rule [15]. The second method, introduced in [19], is polynomial filtering, in which the coefficient of the highest order basis polynomial is reduced by a β fraction. This will dampen high-frequency oscillations and reduce the accumulation of energy in the highest wave numbers. In the present study, all computations are carried out with dealiasing and 5% polynomial filtering ($\beta = 0.05$).

We should emphasize that, in our numerical study, the effect of polynomial filtering is entirely decoupled from the effect of LES modeling. Indeed, in all our numerical tests, when we compared under-resolved simulations (DNS*) with LES results, we always used the same spatial resolution, the same temporal resolution, and the same level of polynomial filtering. Thus, the improvement of the LES results over the DNS* results is entirely due to the LES terms, and not to the polynomial filtering.

3.2 Model Configuration and Parameters

The model setup is similar to that used in [42], which contains a detailed discussion of the boundary conditions, initial conditions and parameters used. In this section, we mainly highlight the differences from the setting used in [42].

The computational domain is $-\frac{L}{2} \le x \le \frac{L}{2}$, $0 \le y \le W$, and $0 \le z \le H$, where $L/H = 2$ and $W/H = 1$. The Froude number, which is a measure of the stratification effects in the flow, is set to $Fr = 2^{-\frac{1}{2}}$. Thus, in this numerical study, we are mainly concerned with

weakly stratified flows. The Peclet number can be written as $Pe = Re\,Pr$, where $Pr = \nu/\kappa$ is the Prandtl number. Corresponding to that of heat and water at room temperature, we take $Pr = 7$. The Reynolds number Re controls the range of turbulent features and interactions in the flow field, and as such, is of great interest. In this study, we consider $Re = 10{,}000$, which corresponds to moderately turbulent flows.

The boundary conditions we use in this study are significantly different from those used in [42]. The main difference is that here we use periodic boundary conditions in *both* horizontal directions, whereas in [42] we used periodic boundary conditions only in one horizontal direction. The motivation for our choice is that in the mathematical developments in the previous sections, the domain considered also has periodic boundary conditions in both horizontal directions. Thus, for both velocity and density perturbation fields, we use the following boundary conditions in both horizontal directions: $u(x,0,z) = u(x,W,z)$; $v(x,0,z) = v(x,W,z)$; $w(x,0,z) = w(x,W,z)$; $\rho'(x,0,z) = \rho'(x,W,z)$; $u(-\frac{L}{2},y,z) = u(\frac{L}{2},y,z)$; $v(-\frac{L}{2},y,z) = v(\frac{L}{2},y,z)$; $w(-\frac{L}{2},y,z) = w(\frac{L}{2},y,z)$; $\rho'(-\frac{L}{2},y,z) = \rho'(-\frac{L}{2},y,z)$. At the top and bottom, no-flow and free-slip boundary conditions are used for the velocity components (u,v,w), while no-flux (insulation) conditions are used for the density perturbation ρ', i.e., $\frac{\partial u}{\partial \mathbf{n}} = 0$; $\frac{\partial w}{\partial \mathbf{n}} = 0$; $(u,v,w)\cdot\mathbf{n} = 0$; $\frac{\partial \rho'}{\partial \mathbf{n}} = 0$, where $\mathbf{n}$ is the normal to the boundary.

Numerical experiments are carried out at two different resolutions: (i) a fine resolution for the DNS run; and (ii) a coarse resolution for the DNS* (the under-resolved simulation) and all the LES models tested. For the fine resolution, we use $K_x = 32$, $K_y = 16$, $K_z = 16$ equally-spaced elements in x,y,z directions, respectively, and a polynomial order $N = 10$ (corresponding to a number of grid points of $n = (K_xN+1)(K_yN+1)(K_zN+1) = 8{,}320{,}614$). For the coarse resolution, we use $K_x = 16$, $K_y = 8$, $K_z = 8$ equally-spaced elements in x,y,z directions, respectively, and a polynomial order $N = 8$ (corresponding to a number of grid points of $n = (K_xN+1)(K_yN+1)(K_zN+1) = 545{,}025$). It was shown in [42] that the finest resolution used does indeed correspond to DNS, since results do not change once the mesh is further refined. Numerical results at the finest resolution (i.e., DNS) are used as benchmark for all the LES models investigated.

The spatial filter scale α for the Rational and Clark-α LES models is computed as follows: $\alpha = (\Delta x_{max}\Delta y_{max}\Delta z_{max})^{1/3}$, where Δx_{max}, Δy_{max} and Δz_{max} are the maximum distances between Lagrange polynomial points in the spectral element discretization. As shown in Sect. 5.2.4 in [40], in our spectral element model setting, the ratio of the spatial filter scale to the domain height for the coarse (LES) resolution is $\alpha/H \approx \pi/(2K_zN)$, where $N = 8$ and $K_z = 8$. Thus, we find that $\alpha/H \approx 0.025$. On the other hand, from (40) in [40], the ratio of the Ozmidov scale ℓ_O to the domain height for the coarse (LES) resolution can be estimated as $\ell_O/H \approx 0.2$. Thus, the Ozmidov scale ℓ_O, which is the energy-containing scale in stratified mixing, is about 8 times larger than the spatial filter scale α. This implies that all the LES models have a spatial filter scale that is small enough to resolve the Ozmidov scale ℓ_O.

Another major difference from our previous study in [42] is the total integration time employed. In the present study, the non-dimensional integration time is $T = 46$, which is more than three times larger than the integration time used in [42]. Thus, the integration time is adequate for multiple sloshings, for the bulk of the turbulent mixing to take place, and for differences among numerical experiments to become apparent. In addition, in the current numerical investigation we are able to assess whether long time integration has an effect on the quality of the results produced by the LES models.

All experiments were run on Virginia Tech's SystemX, based on 2200 Apple G5 processors with 2.3 GHz and InfiniBand interconnect. For the DNS run, 192 processors were used and the CPU time was about 100 hours. For the LES runs, 16 processors were used and the CPU time was about 10 hours.

The accuracy of the LES models is evaluated through *a posteriori* testing. The main measure used is the background/reference potential energy (RPE), which represents an appropriate measure for mixing in an enclosed system [51]. RPE is the minimum potential energy that can be obtained through an adiabatic redistribution of the water masses. To compute RPE, we use the probability density function approach introduced by [49]. Specifically, we split the density perturbation field into 51 bins at each time step, and integrate:

$$RPE := gLW \int_0^H \rho'(z_r) z_r \, dz_r,$$

where $z_r(\rho')$ is the height of fluid of density ρ' in the minimum potential energy state. It is convenient to use the non-dimensional background potential energy

$$RPE^*(t^*) := \frac{RPE(t^*) - RPE(0)}{RPE(0)}, \tag{8}$$

which shows the relative increase of the RPE with respect to the initial state by mixing. Further discussion of the energetics of the lock-exchange problem can be found in [40–42].

Finally, the parameters of the LES models are chosen based on the parameter study conducted in [42].

3.3 Numerical Results

Results of numerical simulations with the four LES models (summarized for clarity in Table 1) are presented in Figs. 1, 2, and 3.

To illustrate the complexity of the mixing process that we investigate, in Fig. 1 we present snapshots of DNS for the density perturbation ρ' at different times. The DNS time evolution of the density perturbation will represent the benchmark for all four LES models tested in this section.

In Fig. 2, we present snapshots of the density perturbation ρ' at $t = 3.0$ for four models: horizontal Rational LES model, horizontal Clark-α LES model, DNS, and DNS* (under-resolved numerical simulation). Notice that all four numerical models produce results that

Table 1 List of the LES models investigated in this study

isotropic Rational (RLES)	$\boldsymbol{\tau}_{\text{RLES}} = \left(\mathrm{I} - \frac{\alpha^2}{4\gamma}\Delta\right)^{-1}\left(\frac{\alpha^2}{2\gamma}\nabla\mathbf{w}\nabla\mathbf{w}^T\right)$
	$\boldsymbol{\sigma}_{\text{RLES}} = \left(\mathrm{I} - \frac{\alpha^2}{4\gamma}\Delta\right)^{-1}\left(\frac{\alpha^2}{2\gamma}\nabla\mathbf{w}\nabla\rho'\right)$
isotropic Clark-α (Clark-α)	$\boldsymbol{\tau}_{\text{Clark-}\alpha} = \left(\mathrm{I} - \frac{\alpha^2}{2\gamma}\Delta\right)^{-1}\left(\frac{\alpha^2}{2\gamma}\nabla\mathbf{w}\nabla\mathbf{w}^T\right)$
	$\boldsymbol{\sigma}_{\text{Clark-}\alpha} = \left(\mathrm{I} - \frac{\alpha^2}{2\gamma}\Delta\right)^{-1}\left(\frac{\alpha^2}{2\gamma}\nabla\mathbf{w}\nabla\rho'\right)$
horizontal Rational (hRLES)	$\boldsymbol{\tau}_{\text{hRLES}} = \left(\mathrm{I} - \frac{\alpha^2}{4\gamma}\Delta_h\right)^{-1}\left(\frac{\alpha^2}{2\gamma}\nabla_h\mathbf{w}\nabla_h\mathbf{w}^T\right)$
	$\boldsymbol{\sigma}_{\text{hRLES}} = \left(\mathrm{I} - \frac{\alpha^2}{4\gamma}\Delta_h\right)^{-1}\left(\frac{\alpha^2}{2\gamma}\nabla_h\mathbf{w}\nabla_h\rho'\right)$
horizontal Clark-α (hClark-α)	$\boldsymbol{\tau}_{\text{hClark-}\alpha} = \left(\mathrm{I} - \frac{\alpha^2}{2\gamma}\Delta_h\right)^{-1}\left(\frac{\alpha^2}{2\gamma}\nabla_h\mathbf{w}\nabla_h\mathbf{w}^T\right)$
	$\boldsymbol{\sigma}_{\text{hClark-}\alpha} = \left(\mathrm{I} - \frac{\alpha^2}{2\gamma}\Delta_h\right)^{-1}\left(\frac{\alpha^2}{2\gamma}\nabla_h\mathbf{w}\nabla_h\rho'\right)$

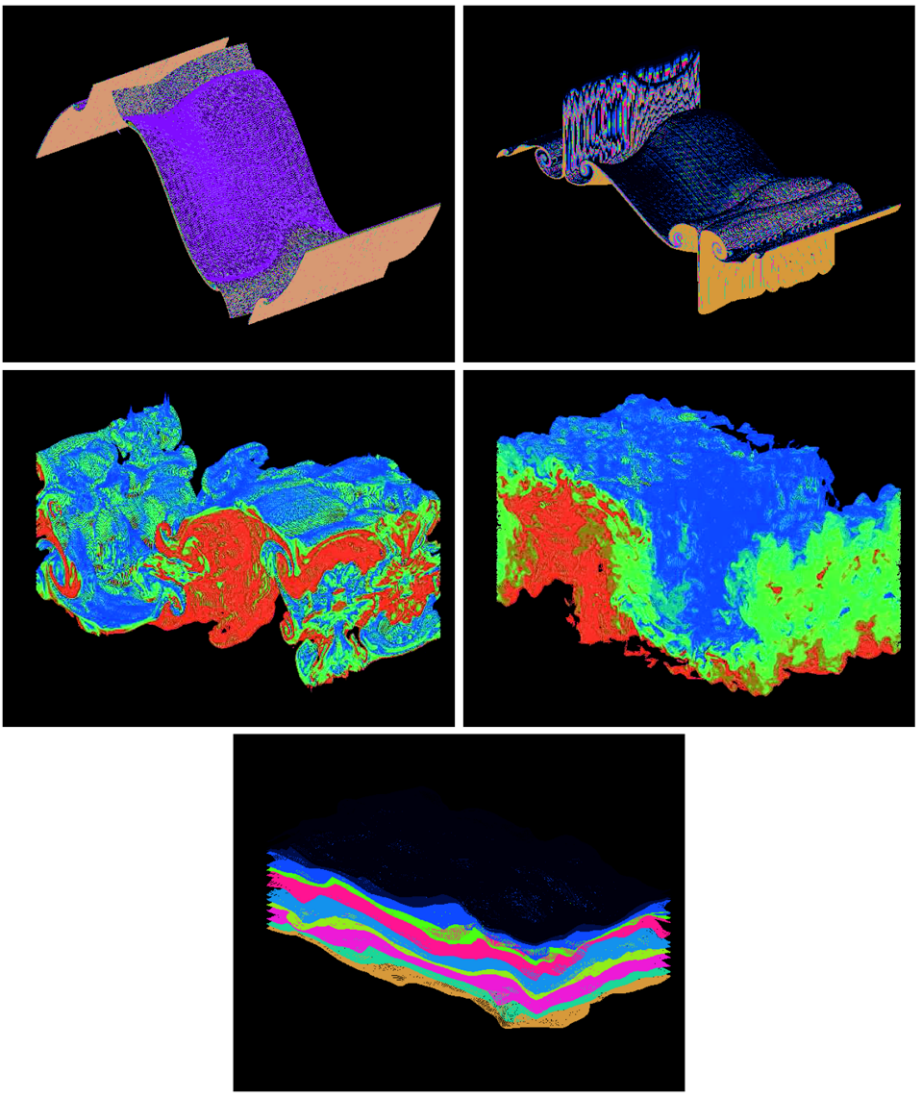

Fig. 1 (Color online) Density perturbation snapshots. DNS at: (**a**) $t = 0.8$; (**b**) $t = 1.2$; (**c**) $t = 3.0$; (**d**) $t = 5.0$; and (**e**) $t = 45.0$

look similar. This is, however, deceiving, since in [42] it was shown that the under-resolved numerical simulation DNS* does not capture accurately the turbulent mixing in the lock-exchange system. Thus, for a reliable assessment of the four LES models investigated in this section, alternatives to a direct visual inspection of the time evolution of the density perturbation must be utilized.

The main measure used in the assessment of the accuracy of the LES models in predicting mixing in the lock-exchange problem is the non-dimensional background potential energy RPE defined in (8), cf. [51]. In Fig. 3 we investigate the ability of the four LES models to reproduce the RPE curve produced by DNS runs. The comparison criterion is

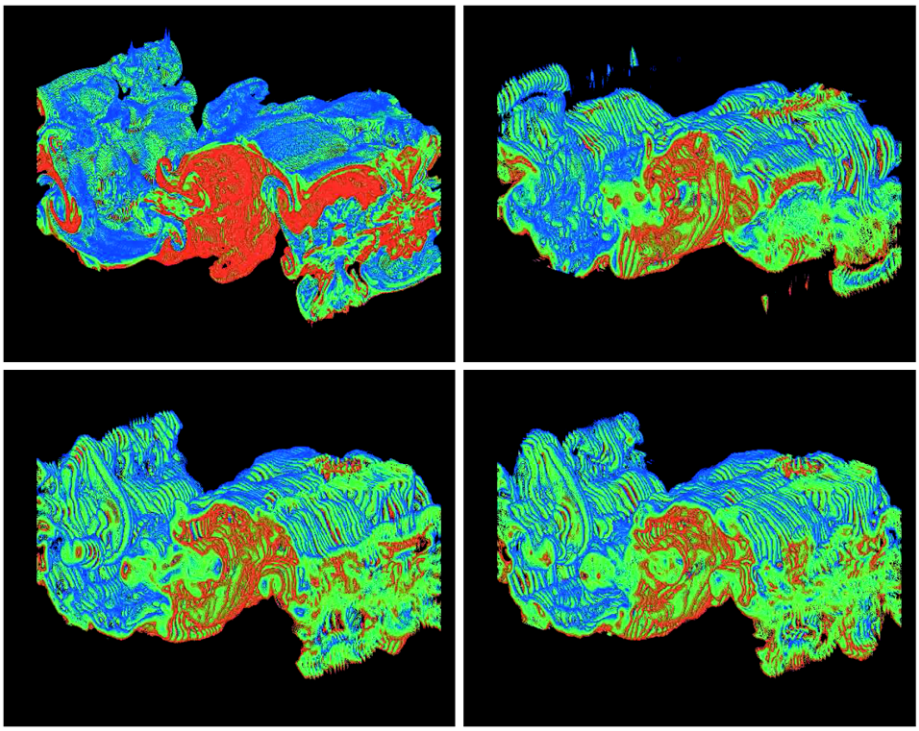

Fig. 2 (Color online) Density perturbation snapshots. (**a**) DNS; (**b**) DNS* (under-resolved numerical simulation); (**c**) horizontal Clark-α LES model; and (**d**) horizontal Rational LES model

simple: the closer the LES RPE curve is to the benchmark DNS RPE curve, the better the LES model. Thus, in contrast to Fig. 2, the RPE curves in Fig. 3 clearly quantify the performance of the LES models tested. RPE curves for six models are plotted in Fig. 3: DNS (green); DNS*—under-resolved simulation—(red); isotropic Rational LES model (blue); horizontal Rational LES model ($+++$); isotropic Clark-α LES model ($\times\times\times$); and horizontal Clark-α LES model (000). The best results (i.e., closest to the RPE curve yielded by the DNS) are obtained with the horizontal Clark-α LES model. The horizontal Rational LES model also performs well—it gives results that are close to those from the horizontal Clark-α LES model, especially at the beginning of the simulation, when turbulent mixing is the most active. In the second part of the simulation, the quality of the RPE curve produced by the horizontal Rational LES model degrades, although toward the end of the simulation it improves again. Nevertheless, overall the horizontal Rational and Clark-α LES models perform *significantly* better than their standard isotropic counterparts (and clearly better than the under-resolved numerical simulation DNS*). Indeed, the isotropic Clark-α LES model yields results that are worse than the DNS* results (i.e., the numerical simulation on the coarse mesh without using any LES model). Thus, the isotropic Clark-α LES model is not appropriate for this setting. The isotropic Rational LES model performs better than DNS* for most of the simulation, but degrades toward the end of the simulation. We emphasize that this behavior was not displayed in our previous studies [41, 42], since there we did not integrate as long in time as in our present study.

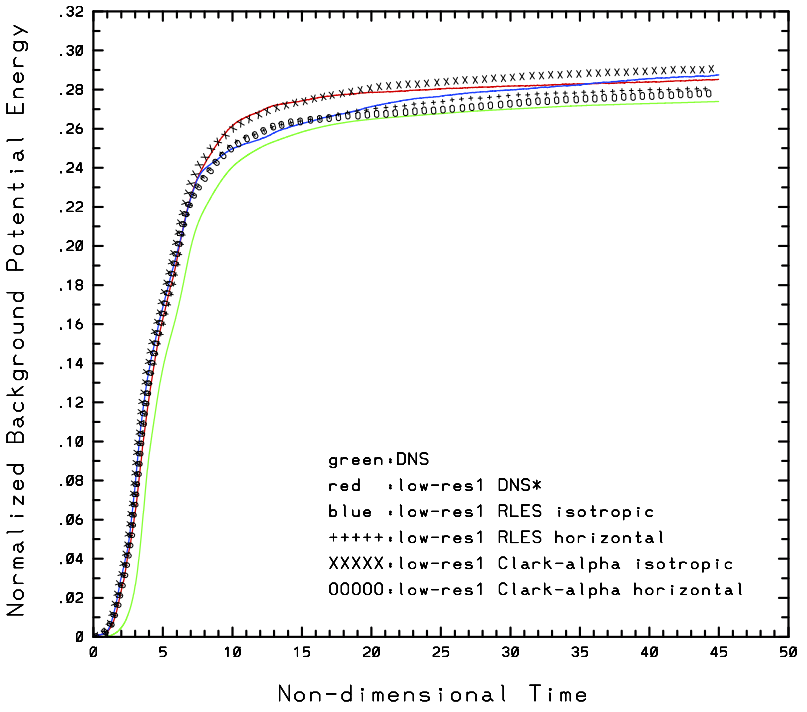

Fig. 3 (Color online) RPE curves: DNS, DNS* (under-resolved numerical simulation), isotropic Clark-α LES model, horizontal Clark-α LES model, isotropic Rational LES model, and horizontal Rational LES model

We note that the DNS results in Fig. 3 have not been filtered. From our previous experience with the lock-exchange problem, filtering the DNS data does not change the overall qualitative results. We believe that this is mainly due to the fact that the spatial filtering radius α is not too large. In realistic ocean flows, where computational resources become utterly scarce, however, one needs to consider a very large filtering radius. In this case, one needs to replace the DNS data in Fig. 3 with its filtered counterpart, where the horizontal filtering is carried out by convolution with the kernel $g_\alpha(\cdot)$ introduced in Sect. 2. We plan to investigate the effect of replacing DNS data with filtered DNS data in a forthcoming study.

4 Conclusions

In this paper, we presented several analytical and numerical results for two new LES models: the horizontal Rational and Clark-α LES models. In the derivation of these two LES models, we employed horizontal spatial filtering instead of the standard isotropic filtering. Thus, the two horizontal LES models could represent appropriate choices for the numerical simulation of turbulent flows that display a high degree of spatial anisotropy. One natural application is mixing in stratified flows, such as those encountered in the ocean. The mathematical results regarding the horizontal Rational and Clark-α LES models were supported by several numerical experiments that showed that both horizontal LES models perform better than their standard, isotropic counterparts in approximating mixing in a 3D lock-exchange problem

at Reynolds number $Re = 10{,}000$. One significant difference from our previous preliminary study [6] is that here we used the anisotropic version of the Helmholtz operator.

The analysis and numerical tests in this report show that the horizontal LES models are promising and may be used to improve the performances of current LES modeling strategies for mixing in stratified flows. These new results open new theoretical and numerical research avenues that we are currently pursuing. The new insight gained from these investigations might be used in the numerical simulation of mixing in realistic oceanic flows.

References

1. Beare, R., MacVean, M., Holtslag, A., Cuxart, J., Esau, I., Golaz, J., Jimenez, M., Khairoutdinov, M., Kosovic, B., Lewellen, D., Lund, T., Lundquist, J., McCabe, A., Moene, A., Noh, Y., Rasch, S., Sullivan, P.: An intercomparison of large-eddy simulations of the stable boundary layer. Bound. - Layer Meteorol. **118**(2), 247–272 (2006)
2. Benjamin, T.B.: Gravity currents and related phenomena. J. Fluid Mech. **31**, 209–248 (1968)
3. Berselli, L.C.: Analysis of an anisotropic approximate deconvolution LES model. Tech. Rep. 5, Dipartimento di Matematica Applicata "U.Dini" (2010)
4. Berselli, L.C., Galdi, G.P., Iliescu, T., Layton, W.J.: Mathematical analysis for the rational large eddy simulation model. Math. Models Methods Appl. Sci. **12**(8), 1131–1152 (2002)
5. Berselli, L.C., Iliescu, T., Layton, W.J.: Mathematics of Large Eddy Simulation of Turbulent Flows. Scientific Computation. Springer, Berlin (2006)
6. Berselli, L.C., Iliescu, T., Özgökmen, T.: Horizontal approximate deconvolution for stratified flows: Analysis and computations. In: Meyers, J., Geurts, B.J., Sagaut, P., Vittoria, S.M. (eds.) Quality and Reliability of Large-Eddy Simulations II. Proceedings of the 2nd Meeting (QLES 2009), held in Pisa, September 9–11, 2009. ERCOFTAC Series. Springer, Berlin (2010)
7. Brezis, H.: Analyse fonctionnelle. Masson, Paris (1983)
8. Britter, R.E., Simpson, J.E.: Experiments on the dynamics of a gravity current head. J. Fluid Mech. **88**, 223–240 (1978)
9. Cantero, M.I., Balachandar, S., Garcia, M., Ferry, J.R.: Direct numerical simulations of planar and cylindrical density currents. J. Appl. Mech. **73**, 923–930 (2006)
10. Cantero, M.I., Lee, J.R., Balachandar, S., Garcia, M.: On the front velocity of gravity currents. J. Fluid Mech. **586**, 1–39 (2007)
11. Cao, C., Holm, D.D., Titi, E.S.: On the Clark-α model of turbulence: global regularity and long-time dynamics. J. Turbul. **6**, Paper 20, 11 pp. (electronic) (2005)
12. Chang, Y., Xu, X., Özgökmen, T.M., Chassignet, E., Peters, H., Fischer, P.: Comparison of gravity current mixing parameterizations and calibration using a high-resolution 3d nonhydrostatic spectral element model. Ocean Model. **10**, 342–368 (2005)
13. Chemin, J.Y., Desjardins, B., Gallagher, I., Grenier, E.: Fluids with anisotropic viscosity. Modél. Math. Anal. Numér. **34**(2), 315–335 (2000). Special issue for R. Temam's 60th birthday
14. Constantin, P., Foias, C.: Navier-Stokes Equations. Chicago Lectures in Mathematics. University of Chicago Press, Chicago (1988)
15. Deville, M., Fischer, P., Mund, E.: High-Order Methods for Incompressible Fluid Flow. Cambridge Monographs on Applied and Computational Mathematics, vol. 9. Cambridge University Press, Cambridge (2002)
16. Dryja, M., Widlund, O.B.: An additive variant of the Schwarz alternating method for the case of many subregions. Technical Report 339, Dept. Computer Science, Courant Institute (1987)
17. Fan, J., Ozawa, T.: Regularity criteria for the 3D density-dependent Boussinesq equations. Nonlinearity **22**(3), 553–568 (2009)
18. Fischer, P.: An overlapping Schwarz method for spectral element solution of the incompressible Navier-Stokes equations. J. Comput. Phys. **133**, 84–101 (1997)
19. Fischer, P., Mullen, J.: Filter-based stabilization of spectral element methods. C. R. Acad. Sci. Paris Sér. I Math. **332**(3), 265–270 (2001)
20. Galdi, G.P., Layton, W.J.: Approximation of the larger eddies in fluid motions. II. A model for space-filtered flow. Math. Models Methods Appl. Sci. **10**(3), 343–350 (2000)
21. Geurts, B.J., Holm, D.D.: Regularization modeling for large-eddy simulation. Phys. Fluids **15**(1), L13–L16 (2003)
22. Hacker, J., Linden, P.F., Dalziel, S.B.: Mixing in lock-release gravity currents. Dyn. Atmos. Oceans **24**(1–4), 183–195 (1996)

23. Hallworth, M.A., Huppert, H.E., Phillips, J.C., Sparks, R.S.J.: Entrainment into two-dimensional and axisymmetric turbulent gravity currents. J. Fluid Mech. **308**, 289–311 (1996)
24. Hallworth, M.A., Phillips, J.C., Huppert, H.E., Sparks, R.S.J.: Entrainment in turbulent gravity currents. Nature **362**, 829–831 (1993)
25. Härtel, C., Meiburg, E., Necker, F.: Analysis and direct numerical simulation of the flow at a gravity-current head. Part 1. Flow topology and front speed for slip and no-slip boundaries. J. Fluid Mech. **418**, 189–212 (2000)
26. Huppert, H.E., Simpson, J.E.: The slumping of gravity currents. J. Fluid Mech. **99**, 785–799 (1980)
27. Iliescu, T., Fischer, P.F.: Large eddy simulation of turbulent channel flows by the rational LES model. Phys. Fluids **15**, 3036–3047 (2003)
28. Iliescu, T., Fischer, P.F.: Backscatter in the rational LES model. Comput. Fluids **33**, 783–790 (2004)
29. Kantha, L.H., Clayson, C.A.: Small Scale Processes in Geophysical Flows. Academic Press, New York (2000)
30. Kosovic, B., Curry, J.: Large eddy simulation study of a quasi-steady, stably stratified atmospheric boundary layer. J. Atmos. Sci. **57**(8), 1052–1068 (2000)
31. Layton, W.J., Lewandowski, R.: On a well-posed turbulence model. Discrete Contin. Dyn. Syst. Ser. B **6**(1), 111–128 (electronic) (2006)
32. Leonard, A.: Energy cascade in large eddy simulations of turbulent fluid flows. Adv. Geophys. **18A**, 237–248 (1974)
33. Lottes, J.W., Fischer, P.F.: Hybrid multigrid/Schwarz algorithms for the spectral element method. J. Sci. Comput. **24**(1), 45–78 (2005)
34. Maday, Y., Patera, A.T.: Spectral element methods for the Navier-Stokes equations. In: Noor, A.K. (ed.) State of the Art Surveys in Computational Mechanics, pp. 71–143. ASME, New York (1989)
35. Maday, Y., Patera, A.T., Rønquist, E.M.: An operator-integration-factor splitting method for time-dependent problems: application to incompressible fluid flow. J. Sci. Comput. **5**(4), 263–292 (1990)
36. Marstorp, L., Brethouwer, G., Johansson, A.: A stochastic subgrid model with application to turbulent flow and scalar mixing. Phys. Fluids **19**, 035107 (2007)
37. Munk, W.: Abyssal recipes. Deep-Sea Res. **13**, 707–730 (1966)
38. Munk, W., Wunsch, C.: Abyssal recipes ii: energetics of tidal and wind mixing. Deep-Sea Res. I **45**, 1977–2010 (1998)
39. Özgökmen, T.M., Fischer, P.F., Duan, J., Iliescu, T.: Three-dimensional turbulent bottom density currents from a high-order nonhydrostatic spectral element model. J. Phys. Oceanogr. **34**(9), 2006–2026 (2004)
40. Özgökmen, T., Iliescu, T., Fischer, P., Srinivasan, A., Duan, J.: Large eddy simulation of stratified mixing in two-dimensional dam-break problem in a rectangular enclosed domain. Ocean Model. **16**, 106–140 (2007)
41. Özgökmen, T., Iliescu, T., Fischer, P.: Large eddy simulation of stratified mixing in a three-dimensional lock-exchange system. Ocean Model. **26**, 134–155 (2009)
42. Özgökmen, T., Iliescu, T., Fischer, P.: Reynolds number dependence of mixing in a lock-exchange system from direct numerical and large eddy simulations. Ocean Model. **30**(2–3), 190–206 (2009)
43. Patera, A.: A spectral element method for fluid dynamics; laminar flow in a channel expansion. J. Comput. Phys. **54**, 468–488 (1984)
44. Rottman, J.W., Simpson, J.E.: Gravity currents produced by instantaneous releases of a heavy fluid in a rectangular channel. J. Fluid Mech. **135**, 95–110 (1983)
45. Shin, J.O., Dalziel, S.B., Linden, P.F.: Gravity currents produced by lock exchange. J. Fluid Mech. **521**, 1–34 (2004)
46. Simpson, J.E.: The dynamics of the head of a gravity current advancing over a horizontal surface. J. Fluid Mech. **94**, 477–495 (1979)
47. Stolz, S., Adams, N.A.: An approximate deconvolution procedure for large-eddy simulation. Phys. Fluids **11**(7), 1699–1701 (1999)
48. Thorpe, S.: The Turbulent Ocean. Cambridge University Press, New York (2005)
49. Tseng, Y., Ferziger, J.H.: Mixing and available potential energy in stratified flows. Phys. Fluids **13**, 1281–1293 (2001)
50. Tufo, H.M., Fischer, P.: Fast parallel direct solvers for coarse grid problems. J. Parallel Distrib. Comput. **173**, 431–471 (2001)
51. Winters, K.B., Lombard, P.N., Riley, J.J., D'Asaro, E.A.: Available potential energy and mixing in density-stratified fluids. J. Fluid Mech. **289**, 115–128 (1995)
52. Xu, X., Chang, Y., Peters, H., Özgökmen, T., Chassignet, E.: Parameterization of gravity current entrainment for ocean circulation models using a high-order 3d nonhydrostatic spectral element model. Ocean Model. **14**, 19–44 (2006)